Felsic tuff from Rutland Island – A pyroclastic flow deposit in Miocene-sediments of Andaman-Java subduction complex

Tapan Pal[1,*], Biswajit Ghosh[2,**], Anindya Bhattacharya[3] and S K Bhaduri[4]

[1]*Petrology Division, ER, Geological Survey of India, Kolkata, India.*
[2]*Department of Geology, University of Calcutta, 35 B.C. Road, Kolkata 700 019, India.*
[3]*Andaman Division, Op. WSA, ER, Geological Survey of India, Kolkata, India.*
[4]*Chemical Division, ER, Geological Survey of India, Kolkata, India.*
e-mail: tapanpal_in@yahoo.co.uk
**e-mail: bghosh_geol@hotmail.com*

The bedded felsic tuff exposed in Rutland Island, Andaman, consists of two facies:

- white massive tuff with ill-defined bedding contacts (facies-A) and
- dominantly green tuff exhibiting well-developed turbidite sequence with up-section change from a massive unit to plane laminated units to ripple drift lamination (facies-B).

The felsic tuff is vitric to crysto-vitric in nature and contains broken crystals of quartz, feldspar, biotite and glass shards of different shapes and sizes. The bulk chemistry indicates trachyte to dacite compositional range, and high values of Zr relative to Nb and Y suggest convergent margin tectonic setting of the tuff. Dominance of cuspate shards rather than blocky shards in both the facies indicates subaerial eruption of the pyroclasts. Recurrence of turbidites as well as good sorting of crystals and glass suggest that subaerially erupted ash was transported in subaqueous condition. The bed pattern supports rapid deposition of facies-A from high concentration turbidity flow whereas facies-B could be produced by decrease in grain size and suspended-load fallout rate of turbidity current. Regional correlation suggests that felsic volcanism in Sumatra was the source for such early Miocene to middle Miocene tuff.

1. Introduction

The Rutland Island belonging to the Andaman and Nicobar group of islands in Bay of Bengal is part of the Burma-Andaman-Java subduction complex. Major tectono-stratigraphic elements in these islands striking N–S are approximately parallel to the trend of the Java Trench. The islands comprise Cretaceous ophiolite slices, Tertiary sediments and Quaternary volcanic (figure 1) representing different tectonic elements of subduction complex viz., outer arc, fore-arc and inner arc (Pal *et al* 2003, 2007).

The Mio-Pliocene sediments containing deep marine fossils form an important stratigraphic subdivision within the 3150-meter thick Tertiary sedimentary succession (Roy 1983). A stratigraphic name, 'Archipelago Group' has been coined by earlier workers for these Mio-Pliocene sediments since these occur predominantly in the Ritcheis Archipelago (cf. Ray 1982). The Archipelago Group constitutes a thick sequence of tuff beds along with calcareous and non calcareous sediments. A few studies have so far been carried out on volcanics of this Mio-Pliocene stratigraphic unit (e.g., Pawde and Ray 1963; Srinivasan 1988,
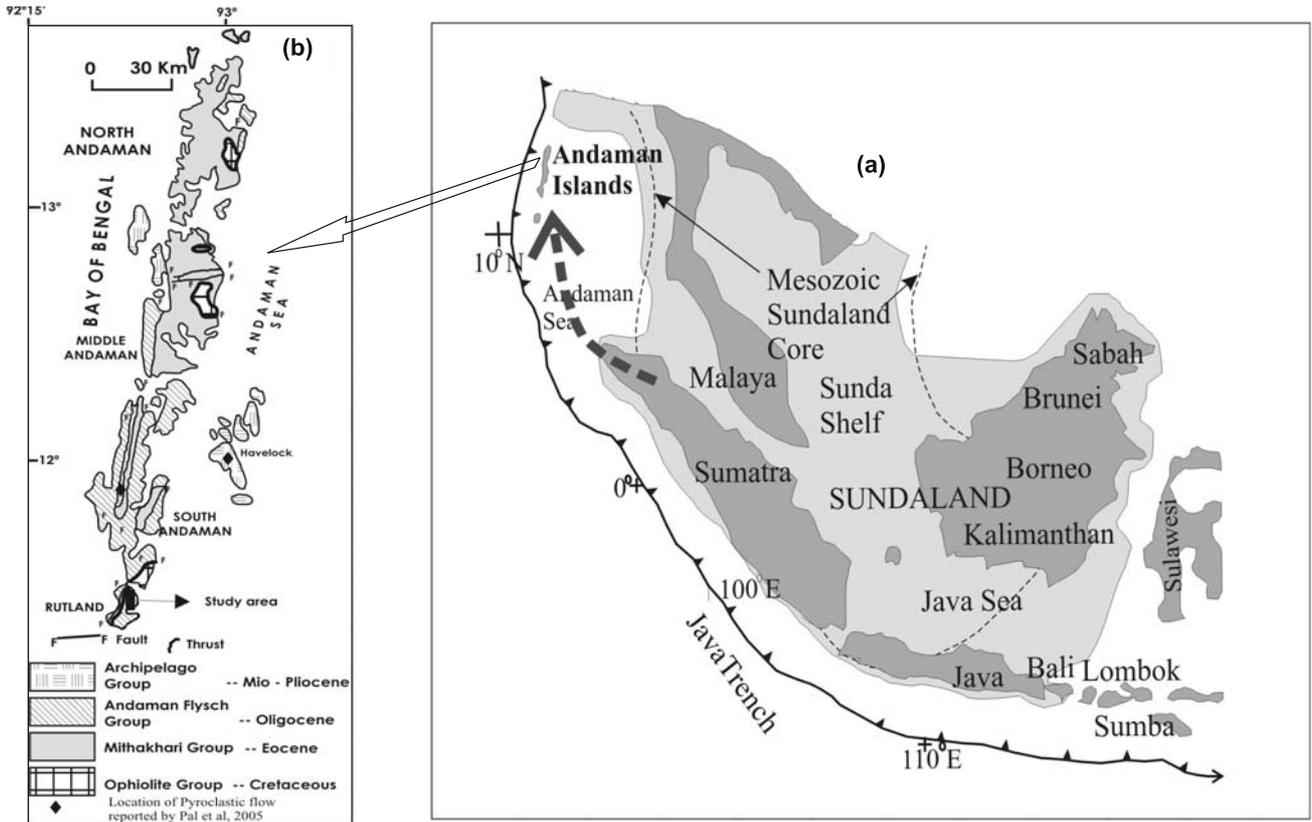
Figure 1. **(a)** Regional geographical features of the Java-Andaman-Burma trench (after Hall 2002; supply of tuff from Sumatra to Andaman islands is indicated by broken line with arrow heads, **(b)** Generalized geological map of Andaman Islands showing distribution of ophiolite and sedimentary units with their stratigraphic relation.

Pal *et al* 2005). We here record the felsic volcanic event from the 'Archipelago Group' sediments of Rutland Island which was earlier recognized as claystone of uncertain origin. Detailed features of volcanogenic events from Tertiary sediments from different islands of Andaman and Nicobar would help to build up local stratigraphy and regional tectonics. Extensive volcanic activity has been reported from early Miocene onwards in Sumatra-Java-Sulewasi and Sundaland areas (cf. Hall 2002). The mineralogical and chemical characterisation of the felsic tuff from the main Andaman and Havelock islands was carried out earlier (Pal *et al* 2005) but the plausible sources and their tectonic correlation in respect of Mio-Pliocene volcanics of south east Asia was not attempted before. The nature and source of eruption and depositional history of the volcanogenic sequence both in time and space needs sincere attention for the evolution of the arc system in the Andaman and Nicobar islands in terms of regional tectonics. Furthermore, scarcity of literature on characterization of the tuff beds from Andaman-Java subduction complex hinders the understanding of the evolutionary history of the arc systems with geologic time.

The bed pattern of Rutland tuff shows features of pyroclastic flow deposit. But recognition of tuff

interbedded with sediments, either as subaerial or subaqueous origin, is often difficult in the rock record but can be differentiated from petrography and mode of occurrences (cf. Cas and Wright 1987). The depositional features of this pyroclastic flow will help to correlate it with the pyroclastic deposits recorded elsewhere in this subduction complex.

The present study has two components viz.,

- characterization of the felsic pyroclastics by field disposition and petrography from hitherto unknown Rutland Island, and
- speculation on the nature of eruption, mode of transport, deposition, and possible tectonic correlation with time and space in terms of regional tectonics of the Burma–Java subduction complex.

2. Mode of occurrence of Rutland tuff

The N–S trending beds of felsic tuff occur in fault contact with Andaman Flysch Group of sediments in the western part and with Mithakhari Group of sediments in the eastern part of Rutland Island. The tuff beds can be grouped into two facies on the basis of colour, bedding character,

primary sedimentary structure, composition, sorting of framework grains and glass alteration. Facies-A is represented by white massive tuff with ill-defined bedding contacts and facies-B comprises dominantly of green tuff with intercalation of white tuff showing well-defined bedding/lamination. The white coloured facies-A is apparently massive and has uniform physical character with crude tabular bed form. The beds are often amalgamated with poorly defined bedding contacts. The massive beds of this facies have indistinct stratification and do not show any scouring base. The massive tuff shows ill-defined parallel stratification towards the top.

The bed sequence of facies-B shows greenish white colour and lateral variation in bed thickness. The tuff beds of this facies show repetitive turbidite units with individual unit showing a change in bed form from a massive unit with a scoured base (U-shaped contact) to plane laminated unit having low angle cross laminations to units with ripple drift lamination occasionally with convolute laminations (figure 2a) which is followed by thin parallel lamination. The beds are usually N–S trending with moderate to steep dips.

3. Petrography

Facies-A is vitric tuff and contains 2–4% phenocrystic crystals along with delicately shaped glass shards. On the other hand, the bedded tuff of facies-B is crysto-vitric and contains 8–10% crystals and numerous glass shards. Facies-A contains 2–3% quartz, 1–2% feldspar, < 1% biotite, on the other hand facies-B contains 6–7% quartz, 2–3% feldspar and 2–3% mica. Opaques are more common in facies-B than in facies-A.

3.1 *Phenocrystic crystals*

In both the facies quartz grains are represented by broken euhedral crystals and acicular to triangular to rectangular grains often showing embayment. Both plagioclase and alkali feldspars are present. The alkali feldspar is usually rectangular to equant shaped and rarely with triangular to very irregular outline. Plagioclase is usually lath shaped and predominates over the alkali feldspar. In both the facies, plagioclases are relatively fresh whereas alkali feldspars show sericitisation along cleavage planes. Biotite crystals occurring as flakes to needle to very irregular shape are more prevalent in facies-B than in facies-A.

3.2 *Glass shards*

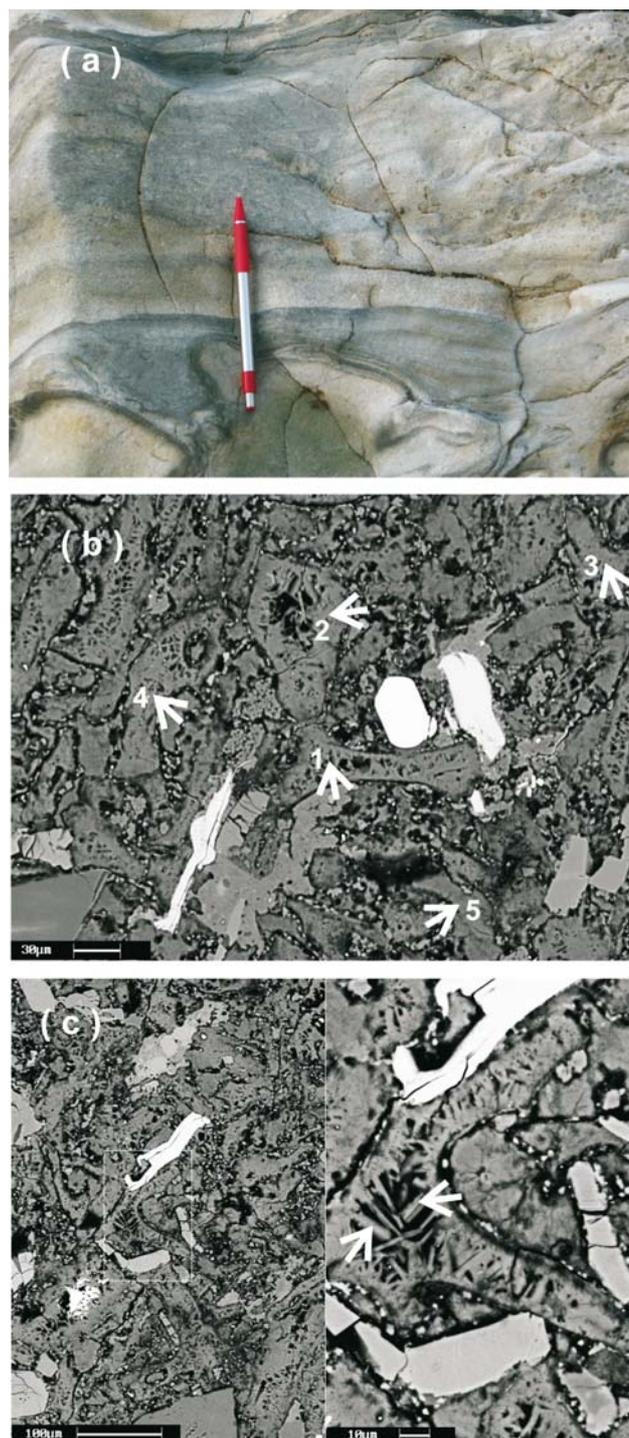Glass shards in both the facies show different shapes varying from platy, bicuspate, tricuspate,

Figure 2. **(a)** Photographs of Rutland tuff (facies-B) showing change from massive beds to plane laminations to convolute laminations, **(b)** photomicrograph showing phenocrystic crystals and typical shapes of glass shards in Rutland tuff. Arrows with numbers indicate different shapes viz., 1 – cuspate, 2 – spindle, 3 – platy, 4 – sickle, 5 – crescent shaped, **(c)** backscattered image showing growth of needle shaped zeolite (shown by arrow) from the wall of a cuspate shard.

crescent to spindle shape (figure 2b). Owing to the presence of different glass shards, the tuff can be grouped into type-5 of Wohletz (1983). Alteration

Table 1. *Electron microprobe analyses of glass shard.*

	Green tuff								
Sample no.	35a	35a	35a	35a	35a	35a	35a	35a	35a
SiO_2	62.83	65.59	70.35	68.16	67.85	68.90	62.40	64.29	62.39
TiO_2	0.02	0.00	0.01	0.01	0.00	0.00	0.03	0.00	0.00
Al_2O_3	11.22	12.02	13.37	12.8	12.58	13.40	11.80	12.18	11.96
FeO	0.27	0.01	0.00	0.06	0.10	0.11	0.00	0.05	0.00
MgO	0.76	0.36	0.40	0.34	0.35	0.44	0.34	0.41	0.43
CaO	0.82	0.40	0.67	0.46	0.35	0.64	0.33	0.50	1.02
Na_2O	4.50	3.83	1.30	2.53	2.05	2.95	3.23	4.24	4.95
K_2O	6.01	5.29	4.09	5.20	5.00	5.00	5.37	5.83	5.87
Total	86.43	87.50	90.19	89.56	88.28	91.40	83.50	87.50	86.62

Note: Analysis was done using CAMECA SX100 Electron Probe Micro Analyzer at 15 kV, 12 nA at 1 μm diameter. The calibration was done against the natural mineral standards supplied by BRGM, France using PAP matrix correction.

Table 2. *Whole rock major element analyses of Rutland tuff (in wt%).*

	Facies-A		Facies-B	
Sample no.	38A	40	35A	36
SiO_2	70.01	68.97	68.80	65.23
Al_2O_3	13.40	13.94	11.90	11.30
$Fe_2O_3(t)$	0.70	0.52	0.85	0.80
MnO	0.02	0.02	0.07	0.06
MgO	1.21	1.17	1.28	1.35
CaO	2.18	2.04	0.60	0.49
Na_2O	0.45	0.32	3.69	3.63
K_2O	2.51	2.34	4.06	4.30
TiO_2	0.12	0.14	0.12	0.11
L.O.I. $(-H_2O)$	9.40	10.54	8.62	12.72
Rb	78	64	27	20
Sr	1922	1653	344	293
Y	14	13	18	17
Zr	249	196	98	82
Nb	< 5	< 5	< 5	< 5
U	< 3	–	< 3	4
Th	12	–	19	10
Ni	< 5	< 5	< 5	< 5
Co	14	12	27	25
Cr	< 5	< 5	< 5	< 5

Note: Analysis was done on fused glass discs by wave length dispersive XRF spectrometer (Panalytical Magix 2424 with End window Rh tube) at 30–60 kV and 40–100 mA conditions for bulk major and trace elements. Natural standards supplied by United States Geological Survey and CRPG (France) were used.

of glass shards into zeolite is common in both the facies but more prevalent in facies-A. Usually needle shaped zeolite crystals grow either from the wall or from the centre of the shards (figure 2c). Sometimes the platy crystals of zeolite also grow from the wall of the shards. Glass shards show a range of chemical composition from trachyte and dacite (table 1).

4. Whole rock geochemistry

The major oxide values were normalised to 100% anhydrous since the tuff samples contain an appreciable amount of adsorbed water (table 2). The silica value shows a narrow range (67.21% to 68.73%) for both facies whereas the total alkali content ($Na_2O + K_2O$) varies widely.
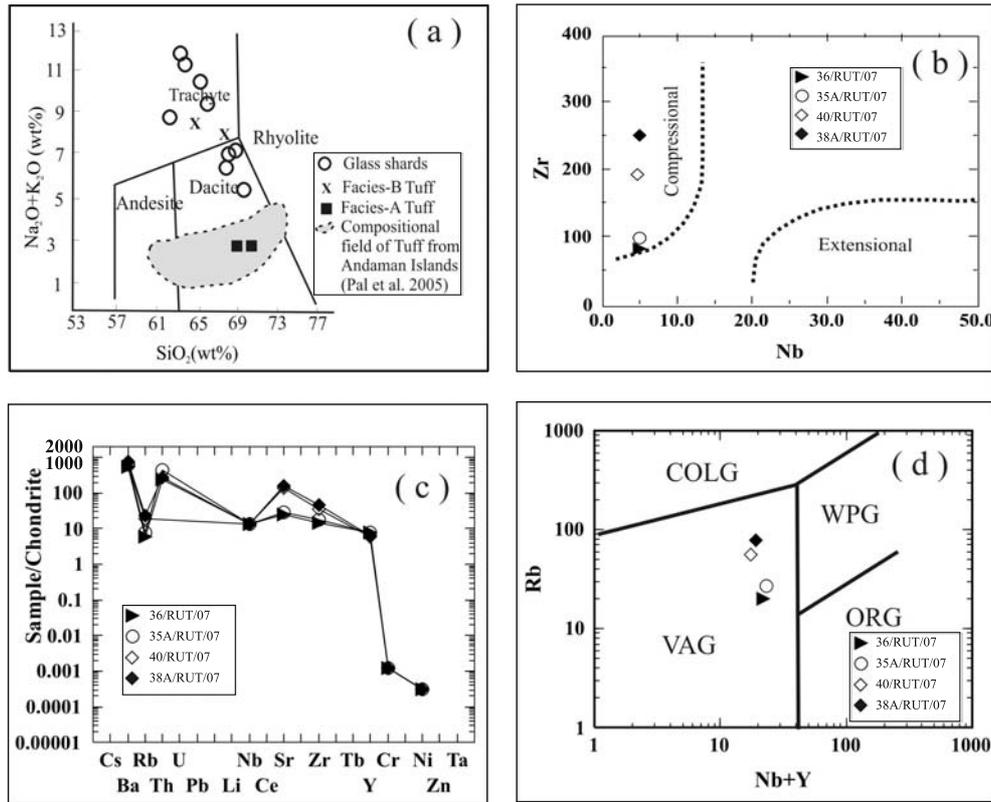
Figure 3. Chemical composition of Rutland tuff: **(a)** total alkali-silica diagram showing trachyte to dacite composition of tuff and glass shards (after Le Bas *et al* 1986), **(b)** trace element distribution normalized against chondrite showing enriched LILE pattern, **(c)** Zr–Nb plot of Rutland tuff showing convergent plate margin set up (after Loomis *et al* 1994), **(d)** Rb–(Y + Nb) plot of indicating the volcanic arc origin (after Pearce *et al* 1984). VAG: volcanic arc granite, ORG: ocean ridge granite, WPG: within plate granite, COLG-syn: collision granite.

Compositionally facies-A tuff falls in dacite field but the facies-B tuff falls in the overlapping field of trachyte and dacite similar to glass shards (figure 3a). Facies-A tuffs have significantly higher values of LILE (e.g., Rb, Ba, Sr) than the facies-B (table 2). The HFSE (Nb, Zr) content shows more or less consistent values. The trace element distribution for both the facies shows it to be enriched in LILE compared to chondrite (figure 3b). In Rb vs. (Y + Nb) compositional diagram, both the facies show the volcanic arc setting (figure 3c) (Pearce *et al* 1984) and Zr–Nb discrimination plot (figure 3d) corresponds with convergent plate margin setting (cf. Loomis *et al* 1994).

5. Discussion and conclusion

5.1 *Nature of eruption, transport and deposition*

The cuspate, curved, v-shaped and crescent glass shards are the fragments of elongate, thin pipe-shaped bubble wall vesicles (cf. Fisher and Schmincke 1984) and are preferably produced in subaerial rather than in subaqueous eruption (Heiken and Wohletz 1985). The absence of the features of phreatomagmatic eruption e.g., blocky/angular glass shards, pumice and welding texture is also not supportive of subaqueous eruption (Heiken 1972; Heiken and Wohletz 1985). Despite their origin in subaerial eruption, the scoured base, normal size grading, good sorting producing crystal rich and glass rich layers in Rutland tuff beds supports their transport in subaqueous condition rather than in subaerial condition (Wright and Mutti 1981; Cashman and Fiske 1991; Cousineau 1994; White 2000). The glass shards of subaerial eruption were possibly transported in cold condition to maintain their original shapes (cf. Cas and Wright 1987; Cousineau 1994). It could therefore, be summarized that the ash of subaerial eruptions entered into the sea and was transported to form subaqueous deposits (cf. Cas and Wright 1987; Whitham 1989; Sigurdsson *et al* 1991).

The massive beds showing poor stratification corresponding to facies-A could be produced by rapid deposition from subaqueous and high concentration turbidity currents (Walker 1978).

The ill-defined parallel stratification towards the top of the sequence is caused due to high suspended-load fallout rate (Lowe 1988). On the other hand, the sequence of tuff beds of facies-B exhibiting Bouma cycles with up-section change from a massive unit with a scoured base to plane laminated units to ripple drift lamination is caused by a decrease in grain size and suspended-load fallout rate (Stix 1991; Cousineau 1994) in turbidity current regime (cf. Cousineau 1994). The graded base and other current structures of facies-B can be produced from low concentration current in limited turbulent flow (cf. Middleton and Hampton 1973; Wright and Mutti 1981).

5.2 *Tectonic correlation*

The higher concentration of Ba and Sr relative to Rb as well as low Rb/Sr and Rb/Ba ratios could be linked to the dominance of plagioclase over alkali feldspar in fractionation path (cf. Anderson *et al* 2000). High Zr/Nb and Zr/Y ratios of Rutland tuff show their lineage to convergent margin tectonic setting. In this terrain, subduction of Indian plate initiated during Cretaceous time (Curray and Moore 1974) and then it may be surmised that inner arc volcanoes were the probable source for Miocene felsic magma. Apart from Miocene sediments no such volcanic events are recorded in Eocene–Oligocene sediments. In the eastern part of the Andaman and Nicobar Islands, the inner arc system developed during Quaternary, as represented by Barren and Narcondum volcanoes. The trachytic-dacitic volcanism usually involves contamination of continental crust. In the Andaman area subduction is an ocean–ocean subduction and no continental crust has been recorded. Furthermore, the tuff beds in the Rutland Island records the product of distal turbidites without any proximal facies. In submarine conditions the finer pyroclastics could be transported to very long distances and in such cases this felsic volcanics could be derived from a distant source.

Felsic volcanism during Miocene age has also been reported from the south to southeastern side of the subduction complex i.e., Sumatra-Java Arc and also from the eastern side i.e., Sundaland shelf. At both Sumatra and Java, the arc underlain by continental crust of Permo-Carboniferous age (Smyth *et al* 2007) records the major felsic volcanic activity during early Miocene (McCourt *et al* 1996). On the other hand, volcanic activity in arc sector between Java and Sumba arc was absent during early to middle Miocene (Hall 2002, 2009). In Sundaland Shelf during Miocene time widespread subsidence was accompanied by volcanic activity. But this non-arc volcanic activity was restricted at middle to late Miocene rather than early to middle Miocene time (Hall 2002, 2009). In Bali, Lombok and Sumba extensive volcanism was recorded during late Miocene to Pliocene time (Simandjuntak and Barber 1996). Hence the Sumatra arc recording volcanic activity during early to middle Miocene time along with continental crust below it, could be the plausible source for dacitic to trachytic volcanics in the Rutland Island and adjoining Andaman Islands (figure 1a)

Extensive felsic magmatism in this subduction zone during Miocene time could be linked to the rotation of Sumatra block from 20 Ma, after that period the subduction hinge retreated towards the Indian Ocean side and the mantle wedge above the subducting plate was replenished (cf. Hall 2002, 2009). On the other hand in the arc sector between Java and Sumba arc activity was absent because of counterclockwise rotation of Sundaland leading to the termination of magmatism in that part of the complex (Hall 2002, 2009).

References

Anderson A T, Davis A M and Lu F 2000 Evolution of Bishop tuff rhyolitic magma based on melt and magnetite inclusions and zoned phenocrysts; *J. Petrol.* **44** 449–473.

Cas R A F and Wright J V 1987 Volcanic successions (London: Allen & Unwin) p. 528.

Cashman K V and Fiske R S 1991 Fallout of pyroclastic debris from submarine volcanic eruption; *Science* **253** 275–280.

Cousineau P A 1994 Subaqueous pyroclastic deposition in an Ordovician forearc basin: An example from the Saint-Victor formation, Quebec Appalachians, Canada; *J. Sed. Res.* **A64** 867–880.

Curray J R and Moore D G 1974 Sedimentary and tectonic processes in the Bengal deep sea fan and geosyncline; In: *The geology of continental margins* (eds) Burke C A and Drake C L (New York: Springer) 617–627.

Fisher R V and Schmincke H U 1984 Volcaniclastic sediment transport and deposition; In: *Sediment transport and depositional processes* (ed) Pye K (Oxford: Blackwell Scientific Publications) 351–388.

Hall R 2002 Cenozoic geological and plate tectonic evolution of SE Asia and the SW Pacific: Computer-drafted reconstructions, model and animations; *J. Asian Earth Sci.* **20** 353–431.

Hall R 2009 Hydrocarbon basins in SE Asia: Understanding why they are there; *Pet. Geosci.* **15** 131–146.

Heiken R 1972 Morphology and petrography of volcanic ashes; *Bull. Geol. Soc. Amer.* **83** 1961–1988.

Heiken G and Wohletz K 1985 Volcanic ash (Berkeley: University of California Press) p. 256.

Le Bas M J, Maitre R W, Streckeisen A and Zanettin B 1986 A chemical classification of volcanic rocks based on the total alkali-silica diagram; *J. Petrol.* **27** 745–750.

Loomis J, Weaver B and Blatt H 1994 Geochemistry of Mississippian tuffs from the Ouachita mountains, and implications for the tectonics of the Ouachita Orogen, Oklhoma and Arkansas; *Bull. Geol. Soc. Amer.* **106** 1158–1171.

Lowe D R 1988 Suspended-load fallout rate as an independent variable in the analysis of current structure; *Sedimentology* **35** 765–776.

McCourt W J, Crow M J, Cobbing E J and Amin T C 1996 Mesozoic and Cenozoic plutonic evolution of SE Asia, evidence from Sumatra, Indonesia; In: *Tectonic evolution of SE Asia* (eds) Hall R and Blundell D J, *Geol. Soc. London Spec. Publ.* **106** 321–325.

Middleton G V and Hampton M A 1973 Sediment gravity flows: Mechanics of flow deposition; *Society of Economic Mineralogy and Paleontology Short course, Anaheim* **1** 1–38.

Pal T, Chakraborty P P, Dutta Gupta T and Singh C D 2003 Geodynamic evolution of the outer arc-forearc belt in the Andaman Islands, the central part of the Burma-Java subduction complex; *Geol. Mag.* **140** 289–307.

Pal T, Duttagupta T, Chakraborty P P and Dasgupta S C 2005 Pyroclastic deposits of Mio-Pliocene age in the Arakan Yoma-Andaman-Java subduction Complex, Andaman Islands, Bay of Bengal, India; *Geochemical Journal* **39** 69–82.

Pal T, Mitra S K, Sengupta S, Katari A, Bandopadhyay P C and Bhattacharya A K 2007 Dacite-andesites of Narcondam volcano in the Andaman Sea – An imprint of magma mixing in the inner arc of the Andaman-Java subduction system; *J. Vol. Geoth. Res.* **168** 93–113.

Pawde M B and Ray K K 1963 On the age of greywackes in south Andaman; *Science and Culture* **30** 279–280.

Pearce J A, Lippard S J and Roberts S 1984 Characteristics and tectonic significance of supra-subduction zone ophiolites; In: *Marginal Basin Geology. Volcanic and associated sedimentary and tectonic processes in modern and ancient marginal basin* (eds) Kokelaar B P and Howells M F, *Geol. Soc. London Spec. Publ.* **16** 77–94.

Ray K K 1982 A review of the geology of Andaman and Nicobar islands; *Geol. Surv. India Misc. Publ.* **42** 110–125.

Roy T K 1983 Geology and hydrocarbon prospects of Andaman and Nicobar; In: *Petroliferous basins of India* (eds) Bhandari L, Venkatachala B S, Kumar R, Swamy S N, Garga P and Srivastava D C (Petrolium Asia Journal, KDMIPE, ONGC, Dehradun) 37–53.

Sigurdsson H, Carey S, Mandeville C and Bronto S 1991 Pyroclastic flows of the 1883 Krakatau eruption: EOS; *American Geophysical Union Transactions* **72** 377–381.

Simandjuntak T O and Barber A J 1996 Contrasting tectonic styles in the Neogene orogenic belts of Indonesia; In: *Tectonic evolution of SE Asia* (eds) Hall R and Blundell D J, *Geol. Soc. London Spec. Publ.* **106** 185–201.

Smyth H R, Hamilton P J, Hall R and Kinny P D 2007 The deep crust beneath island arcs: Inherited zircons reveal a Gondwana continental fragment beneath East Java, Indonesia; *Earth Planet Sci. Lett.* **258** 269–282.

Srinivasan M S 1988 Late Cenozoic sequences of Andaman–Nicobar islands: Their regional significance and correlation; *India J. Geol.* **60** 11–34.

Stix J 1991 Subaqueous, intermediate to silicic-composition explosive volcanism: A review; *Earth Sci. Rev.* **31** 21–53.

Walker R G 1978 Deep-water sandstone facies and ancient submarine fans: Models for exploration for stratigraphic traps; *Bull. Amer. Assoc. Petrol. Geol.* **62** 932–966.

White J D L 2000 Subaqueous eruption-fed density currents and their deposits; *Precamb. Res.* **101** 87–109.

Whitham A G 1989 The behaviour of subaerially produced pyroclastic flows in a subaqueous environment: Evidence from the Roseau eruption, Dominica, West Indes; *Marine Geol.* **86** 27–40.

Wohletz K H 1983 Mechanisms of hydrovolcanic pyroclast formation: Grains size, scanning electron microscopy, and experimental studies; *J. Vol. Geoth. Res.* **17** 31–63.

Wright J V and Mutti 1981 The Dali ash, islands of Rhodes, Greece: A problem in interpreting submarine volcanogenic sediments; *Bull. Vol.* **44** 153–167.